# Measurement of the Electron Neutrino Charged-current Interaction Rate on Water with the T2K ND280 $\pi^0$ Detector

K. Abe,[59] J. Adam,[55] H. Aihara,[58,33] C. Andreopoulos,[51,37] S. Aoki,[34] A. Ariga,[3] S. Assylbekov,[7] D. Autiero,[63] M. Barbi,[49] G.J. Barker,[67] G. Barr,[45] P. Bartet-Friburg,[62] M. Bass,[7] M. Batkiewicz,[14] F. Bay,[11] V. Berardi,[17] B.E. Berger,[7,33] S. Berkman,[5] S. Bhadra,[71] F.d.M. Blaszczyk,[4] A. Blondel,[13] S. Bolognesi,[25] S. Bordoni,[27] S.B. Boyd,[67] D. Brailsford,[26] A. Bravar,[13] C. Bronner,[33] N. Buchanan,[7] R.G. Calland,[33] J. Caravaca Rodríguez,[27] S.L. Cartwright,[53] R. Castillo,[27] M.G. Catanesi,[17] A. Cervera,[16] D. Cherdack,[7] N. Chikuma,[58] G. Christodoulou,[37] A. Clifton,[7] J. Coleman,[37] S.J. Coleman,[8] G. Collazuol,[21] K. Connolly,[68] L. Cremonesi,[47] A. Dabrowska,[14] R. Das,[7] S. Davis,[68] P. de Perio,[61] G. De Rosa,[19] T. Dealtry,[36,45] S.R. Dennis,[67,51] C. Densham,[51] D. Dewhurst,[45] F. Di Lodovico,[47] S. Di Luise,[11] S. Dolan,[45] O. Drapier,[12] K. Duffy,[45] J. Dumarchez,[62] S. Dytman,[46] M. Dziewiecki,[65] S. Emery-Schrenk,[25] A. Ereditato,[3] L. Escudero,[16] T. Feusels,[5] A.J. Finch,[36] G.A. Fiorentini,[71] M. Friend,[15,*] Y. Fujii,[15,*] Y. Fukuda,[40] A.P. Furmanski,[67] V. Galymov,[63] A. Garcia,[27] S. Giffin,[49] C. Giganti,[62] K. Gilje,[55] D. Goeldi,[3] T. Golan,[70] M. Gonin,[12] N. Grant,[36] D. Gudin,[28] D.R. Hadley,[67] L. Haegel,[13] A. Haesler,[13] M.D. Haigh,[67] P. Hamilton,[26] D. Hansen,[46] T. Hara,[34] M. Hartz,[33,56] T. Hasegawa,[15,*] N.C. Hastings,[49] T. Hayashino,[35] Y. Hayato,[59,33] R.L. Helmer,[56] M. Hierholzer,[3] J. Hignight,[55] A. Hillairet,[64] A. Himmel,[10] T. Hiraki,[35] S. Hirota,[35] J. Holeczek,[54] S. Horikawa,[11] F. Hosomi,[58] K. Huang,[35] A.K. Ichikawa,[35] K. Ieki,[35] M. Ieva,[27] M. Ikeda,[59] J. Imber,[12] J. Insler,[38] T.J. Irvine,[60] T. Ishida,[15,*] T. Ishii,[15,*] E. Iwai,[15] K. Iwamoto,[50] K. Iyogi,[59] A. Izmaylov,[16,28] A. Jacob,[45] B. Jamieson,[69] M. Jiang,[35] S. Johnson,[8] J.H. Jo,[55] P. Jonsson,[26] C.K. Jung,[55,†] M. Kabirnezhad,[42] A.C. Kaboth,[26] T. Kajita,[60,†] H. Kakuno,[57] J. Kameda,[59] Y. Kanazawa,[58] D. Karlen,[64,56] I. Karpikov,[28] T. Katori,[47] E. Kearns,[4,†] M. Khabibullin,[28] A. Khotjantsev,[28] D. Kielczewska,[66] T. Kikawa,[35] A. Kilinski,[42] J. Kim,[5] S. King,[47] J. Kisiel,[54] P. Kitching,[1] T. Kobayashi,[15,*] L. Koch,[48] T. Koga,[58] A. Kolaceke,[49] A. Konaka,[56] A. Kopylov,[28] L.L. Kormos,[36] A. Korzenev,[13] Y. Koshio,[43,†] W. Kropp,[6] H. Kubo,[35] Y. Kudenko,[28,‡] R. Kurjata,[65] T. Kutter,[38] J. Lagoda,[42] I. Lamont,[36] E. Larkin,[67] M. Laveder,[21] M. Lawe,[36] M. Lazos,[37] T. Lindner,[56] C. Lister,[67] R.P. Litchfield,[67] A. Longhin,[21] J.P. Lopez,[8] L. Ludovici,[23] L. Magaletti,[17] K. Mahn,[39] M. Malek,[53] S. Manly,[50] A.D. Marino,[8] J. Marteau,[63] J.F. Martin,[61] P. Martins,[47] S. Martynenko,[28] T. Maruyama,[15,*] V. Matveev,[28] K. Mavrokoridis,[37] E. Mazzucato,[25] M. McCarthy,[71] N. McCauley,[37] K.S. McFarland,[50] C. McGrew,[55] A. Mefodiev,[28] C. Metelko,[37] M. Mezzetto,[21] P. Mijakowski,[42] C.A. Miller,[56] A. Minamino,[35] O. Mineev,[28] S. Mine,[6] A. Missert,[8] M. Miura,[59,†] S. Moriyama,[59,†] Th.A. Mueller,[12] A. Murakami,[35] M. Murdoch,[37] S. Murphy,[11] J. Myslik,[64] T. Nakadaira,[15,*] M. Nakahata,[59,33] K.G. Nakamura,[35] K. Nakamura,[33,*] S. Nakayama,[59,†] T. Nakaya,[35,33] K. Nakayoshi,[15,*] C. Nantais,[5] C. Nielsen,[5] M. Nirkko,[3] K. Nishikawa,[15,*] Y. Nishimura,[60] J. Nowak,[36] H.M. O'Keeffe,[36] R. Ohta,[15,*] K. Okumura,[60,33] T. Okusawa,[44] W. Oryszczak,[66] S.M. Oser,[5] T. Ovsyannikova,[28] R.A. Owen,[47] Y. Oyama,[15,*] V. Palladino,[19] J.L. Palomino,[55] V. Paolone,[46] D. Payne,[37] O. Perevozchikov,[38] J.D. Perkin,[53] Y. Petrov,[5] L. Pickard,[53] E.S. Pinzon Guerra,[71] C. Pistillo,[3] P. Plonski,[65] E. Poplawska,[47] B. Popov,[62,§] M. Posiadala-Zezula,[66] J.-M. Poutissou,[56] R. Poutissou,[56] P. Przewlocki,[42] B. Quilain,[12] E. Radicioni,[17] P.N. Ratoff,[36] M. Ravonel,[13] M.A.M. Rayner,[13] A. Redij,[3] M. Reeves,[36] E. Reinherz-Aronis,[7] C. Riccio,[19] P.A. Rodrigues,[50] P. Rojas,[7] E. Rondio,[42] S. Roth,[48] A. Rubbia,[11] D. Ruterbories,[7] A. Rychter,[65] R. Sacco,[47] K. Sakashita,[15,*] F. Sánchez,[27] F. Sato,[15] E. Scantamburlo,[13] K. Scholberg,[10,†] S. Schoppmann,[48] J.D. Schwehr,[7] M. Scott,[56] Y. Seiya,[44] T. Sekiguchi,[15,*] H. Sekiya,[59,†] D. Sgalaberna,[11] R. Shah,[51,45] A. Shaikhiev,[28] F. Shaker,[69] D. Shaw,[36] M. Shiozawa,[59,33] S. Short,[47] Y. Shustrov,[28] P. Sinclair,[26] B. Smith,[26] M. Smy,[6] J.T. Sobczyk,[70] H. Sobel,[6,33] M. Sorel,[16] L. Southwell,[36] P. Stamoulis,[16] J. Steinmann,[48] Y. Suda,[58] A. Suzuki,[34] K. Suzuki,[35] S.Y. Suzuki,[15,*] Y. Suzuki,[33,33] R. Tacik,[49,56] M. Tada,[15,*] S. Takahashi,[35] A. Takeda,[59] Y. Takeuchi,[34,33] H.K. Tanaka,[59,†] H.A. Tanaka,[5,¶] M.M. Tanaka,[15,*] D. Terhorst,[48] R. Terri,[47] L.F. Thompson,[53] A. Thorley,[37] S. Tobayama,[5] W. Toki,[7] T. Tomura,[59] C. Touramanis,[37] T. Tsukamoto,[15,*] M. Tzanov,[38] Y. Uchida,[26] A. Vacheret,[45] M. Vagins,[33,6] G. Vasseur,[25] T. Wachala,[14] K. Wakamatsu,[44] C.W. Walter,[10,†] D. Wark,[51,45] W. Warzycha,[66] M.O. Wascko,[26] A. Weber,[51,45] R. Wendell,[59,†] R.J. Wilkes,[68] M.J. Wilking,[55] C. Wilkinson,[53] Z. Williamson,[45] J.R. Wilson,[47] R.J. Wilson,[7] T. Wongjirad,[10] Y. Yamada,[15,*] K. Yamamoto,[44] C. Yanagisawa,[55,**] T. Yano,[34] S. Yen,[56] N. Yershov,[28] M. Yokoyama,[58,†] J. Yoo,[38] K. Yoshida,[35] T. Yuan,[8] M. Yu,[71] A. Zalewska,[14] J. Zalipska,[42] L. Zambelli,[15,*] K. Zaremba,[65] M. Ziembicki,[65] E.D. Zimmerman,[8] M. Zito,[25] and J. Żmuda[70]

[1] University of Alberta, Centre for Particle Physics, Department of Physics, Edmonton, Alberta, Canada
[2] BMCC/CUNY, Science Department, New York, New York, U.S.A.
[3] University of Bern, Albert Einstein Center for Fundamental Physics, Laboratory for High Energy Physics (LHEP), Bern, Switzerland
[4] Boston University, Department of Physics, Boston, Massachusetts, U.S.A.

[5] University of British Columbia, Department of Physics and Astronomy, Vancouver, British Columbia, Canada

[6] University of California, Irvine, Department of Physics and Astronomy, Irvine, California, U.S.A.

[7] Colorado State University, Department of Physics, Fort Collins, Colorado, U.S.A.

[8] University of Colorado at Boulder, Department of Physics, Boulder, Colorado, U.S.A.

[9] Daresbury Laboratory, Warrington, United Kingdom

[10] Duke University, Department of Physics, Durham, North Carolina, U.S.A.

[11] ETH Zurich, Institute for Particle Physics, Zurich, Switzerland

[12] Ecole Polytechnique, IN2P3-CNRS, Laboratoire Leprince-Ringuet, Palaiseau, France

[13] University of Geneva, Section de Physique, DPNC, Geneva, Switzerland

[14] H. Niewodniczanski Institute of Nuclear Physics PAN, Cracow, Poland

[15] High Energy Accelerator Research Organization (KEK), Tsukuba, Ibaraki, Japan

[16] IFIC (CSIC & University of Valencia), Valencia, Spain

[17] INFN Sezione di Bari and Università e Politecnico di Bari, Dipartimento Interuniversitario di Fisica, Bari, Italy

[18] INFN Sezione di Bari, Bari, Italy

[19] INFN Sezione di Napoli and Università di Napoli, Dipartimento di Fisica, Napoli, Italy

[20] INFN Sezione di Napoli, Napoli, Italy

[21] INFN Sezione di Padova and Università di Padova, Dipartimento di Fisica, Padova, Italy

[22] INFN Sezione di Padova, Padova, Italy

[23] INFN Sezione di Roma and Università di Roma "La Sapienza", Roma, Italy

[24] INFN Sezione di Roma, Roma, Italy

[25] IRFU, CEA Saclay, Gif-sur-Yvette, France

[26] Imperial College London, Department of Physics, London, United Kingdom

[27] Institut de Fisica d'Altes Energies (IFAE), Bellaterra (Barcelona), Spain

[28] Institute for Nuclear Research of the Russian Academy of Sciences, Moscow, Russia

[29] Institute of Particle Physics, Canada

[30] J-PARC, Tokai, Japan

[31] JINR, Dubna, Russia

[32] Kavli IPMU (WPI), the University of Tokyo, Japan

[33] Kavli Institute for the Physics and Mathematics of the Universe (WPI),
Todai Institutes for Advanced Study, University of Tokyo, Kashiwa, Chiba, Japan

[34] Kobe University, Kobe, Japan

[35] Kyoto University, Department of Physics, Kyoto, Japan

[36] Lancaster University, Physics Department, Lancaster, United Kingdom

[37] University of Liverpool, Department of Physics, Liverpool, United Kingdom

[38] Louisiana State University, Department of Physics and Astronomy, Baton Rouge, Louisiana, U.S.A.

[39] Michigan State University, Department of Physics and Astronomy, East Lansing, Michigan, U.S.A.

[40] Miyagi University of Education, Department of Physics, Sendai, Japan

[41] Moscow Institute of Physics and Technology and National Research Nuclear University "MEPhI", Moscow, Russia

[42] National Centre for Nuclear Research, Warsaw, Poland

[43] Okayama University, Department of Physics, Okayama, Japan

[44] Osaka City University, Department of Physics, Osaka, Japan

[45] Oxford University, Department of Physics, Oxford, United Kingdom

[46] University of Pittsburgh, Department of Physics and Astronomy, Pittsburgh, Pennsylvania, U.S.A.

[47] Queen Mary University of London, School of Physics and Astronomy, London, United Kingdom

[48] RWTH Aachen University, III. Physikalisches Institut, Aachen, Germany

[49] University of Regina, Department of Physics, Regina, Saskatchewan, Canada

[50] University of Rochester, Department of Physics and Astronomy, Rochester, New York, U.S.A.

[51] STFC, Rutherford Appleton Laboratory, Harwell Oxford, and Daresbury Laboratory, Warrington, United Kingdom

[52] STFC, Rutherford Appleton Laboratory, Harwell Oxford, United Kingdom

[53] University of Sheffield, Department of Physics and Astronomy, Sheffield, United Kingdom

[54] University of Silesia, Institute of Physics, Katowice, Poland

[55] State University of New York at Stony Brook, Department of Physics and Astronomy, Stony Brook, New York, U.S.A.

[56] TRIUMF, Vancouver, British Columbia, Canada

[57] Tokyo Metropolitan University, Department of Physics, Tokyo, Japan

[58] University of Tokyo, Department of Physics, Tokyo, Japan

[59] University of Tokyo, Institute for Cosmic Ray Research, Kamioka Observatory, Kamioka, Japan

[60] University of Tokyo, Institute for Cosmic Ray Research, Research Center for Cosmic Neutrinos, Kashiwa, Japan

[61] University of Toronto, Department of Physics, Toronto, Ontario, Canada

[62] UPMC, Université Paris Diderot, CNRS/IN2P3, Laboratoire de
Physique Nucléaire et de Hautes Energies (LPNHE), Paris, France

[63] Université de Lyon, Université Claude Bernard Lyon 1, IPN Lyon (IN2P3), Villeurbanne, France

[64] University of Victoria, Department of Physics and Astronomy, Victoria, British Columbia, Canada

[65] Warsaw University of Technology, Institute of Radioelectronics, Warsaw, Poland

[66] University of Warsaw, Faculty of Physics, Warsaw, Poland

[67] *University of Warwick, Department of Physics, Coventry, United Kingdom*
[68] *University of Washington, Department of Physics, Seattle, Washington, U.S.A.*
[69] *University of Winnipeg, Department of Physics, Winnipeg, Manitoba, Canada*
[70] *Wroclaw University, Faculty of Physics and Astronomy, Wroclaw, Poland*
[71] *York University, Department of Physics and Astronomy, Toronto, Ontario, Canada*
[72] *Università di Napoli, Dipartimento di Fisica, Napoli, Italy*
[73] *Università di Padova, Dipartimento di Fisica, Padova, Italy*
[74] *Università di Roma "La Sapienza, Roma, Italy*
[75] *Università e Politecnico di Bari, Dipartimento Interuniversitario di Fisica, Bari, Italy*

This paper presents a measurement of the charged current interaction rate of the electron neutrino beam component of the beam above 1.5 GeV using the large fiducial mass of the T2K $\pi^0$ detector. The predominant poriton of the $\nu_e$ flux ($\sim$85%) at these energies comes from kaon decays. The measured ratio of the observed beam interaction rate to the predicted rate in the detector with water targets filled is $0.89 \pm 0.08$ (stat.) $\pm 0.11$ (sys.), and with the water targets emptied is $0.90 \pm 0.09$ (stat.) $\pm 0.13$ (sys.). The ratio obtained for the interactions on water only from an event subtraction method is $0.87 \pm 0.33$ (stat.) $\pm 0.21$ (sys.). This is the first measurement of the interaction rate of electron neutrinos on water, which is particularly of interest to experiments with water Cherenkov detectors.

## I. INTRODUCTION

This paper reports a measurement of the ratio of the charged current $\nu_e$ event rate relative to the simulation with NEUT [1] event generator, version 4.1.4.2, for neutrino energies above 1.5 GeV in the T2K beam. The interaction rate of electron neutrinos on water has never been measured at the neutrinos energies above 1.5 GeV, or at any other energies. The mean reconstructed energy of the selected neutrinos in the analysis presented in this paper is 2.7 GeV. The $\nu_e$ cross section has been measured on a liquid freon target for energies between 1.5 GeV and 8 GeV by Gargamelle [2] and on $^{12}$C for energies around 32 MeV at LANSCE [3]. Also at lower energies, the anti-electron neutrino interactions have been measured by experiments near nuclear reactors. A review of neutrino cross section measurements can be found in [4].

The T2K experiment [5] was built with the primary goals of precisely determining the oscillation parameter $\theta_{13}$ via electron neutrino appearance, and of the parameters $\theta_{23}$ and $\Delta m_{32}^2$ via muon neutrino disappearance. The predominantly $\nu_\mu$ beam for these measurements is produced at the Japan Proton Accelerator Research Complex (J-PARC) in Tokai. The neutrinos from this beam are observed at a near detector, ND280, which is located 280 m downstream from the production target, where the neutrinos are not expected to have been affected by oscillations. The T2K far detector, Super-Kamiokande (SK), then measures the muon and electron

neutrinos (and anti-neutrinos) after they have undergone a near maximal oscillation.

The oscillation probability for $\nu_\mu \to \nu_e$ depends on the mixing parameter, $\theta_{13}$, and on sub-leading effects that depend on the CP-violating phase, $\delta_{CP}$, and on the mass hierarchy [6]. T2K has already observed the appearance of 28 $\nu_e$ candidate events at the far detector with a 7.3 $\sigma$ significance over a background expectation of $4.92 \pm 0.55$ events for $\theta_{13} = 0$ [7]. The largest irreducible background for the appearance measurement comes from the predicted 3.2 intrinsic $\nu_e$ beam events.

In T2K the $\nu_e$ are expected to represent about 1.2% of the total neutrino flux [8]. The T2K $\nu_\mu$ beam is produced by magnetic focusing of pions and kaons produced by the interaction of a proton beam with a graphite target. The unavoidable $\nu_e$ component comes from the decay of muons from pion decay, and from kaon decay. In any long-baseline neutrino experiment proposed to measure CP violation and precisely measure neutrino oscillation parameters, the $\nu_e$ component of the beam will be the main source of background [9–11].

The measurement of the beam $\nu_e$ charged current (CC$\nu_e$) interactions on a plastic scintillator and water target using ND280 tracker, was reported in[12]. This paper reports a direct measurement of this component of the charged current (CC) neutrino interactions in the ND280 $\pi^0$ Detector (PØD) [13], which is located just upstream of the tracker. In this selection, the majority of the electron neutrinos were produced in kaon decay, and have energies above 1.5 GeV. The PØD detector has water targets that can be filled or emptied. Data were taken both with the targets filled to create a water target (water configuration), and empty to leave just air in place of the water target (air configuration). With data in the two configurations a subtraction analysis obtained the interaction rate just on water.

Similar to the subtraction analysis presented here, a ratio analysis has been conducted by the Minerva collaboration for 2-20 GeV $\nu_\mu$ on C, Fe, and Pb compared

* also at J-PARC, Tokai, Japan
† affiliated member at Kavli IPMU (WPI), the University of Tokyo, Japan
‡ also at Moscow Institute of Physics and Technology and National Research Nuclear University "MEPhI", Moscow, Russia
§ also at JINR, Dubna, Russia
¶ also at Institute of Particle Physics, Canada
** also at BMCC/CUNY, Science Department, New York, New York, U.S.A.

to CH[14]. A subtraction analysis of the Minerva data is presented the thesis of B.G. Tice [15]. Apart from the Minerva measurements, this appears to be the only other use of the subtraction analysis to date in neutrino scattering experiments.

The $\nu_e$ and $\nu_\mu$ come from the same pion to muon to electron decay chain, and lepton universality allows us to constrain the expected rate of $\nu_e$ by measuring the much larger flux of $\nu_\mu$. We refer you to the paper [16] for the T2K beam flux measurement, and further information on recent measurements of the rate of $\nu_\mu$ interactions in the near detectors.

One of the systematic uncertainties in long baseline neutrino oscillation measurements using water Cherenkov detectors comes from model uncertainties in the meson exchange current for C versus for O. Having measurements of neutrino interaction rates on water is therefore important. For a recent review of $\nu_\mu$ cross section measurements on various nuclear targets we refer the reader to the PDG[17]. The only measurements of $\nu_\mu$ neutrino interactions on water were reported by the K2K experiment for quasi-elastic interactions [18], and for reactions resulting in pions in the final state [19–22].

The paper is organized as follows. In Section II the PØD detector, used to do the measurement is described. The electron selection, and expected backgrounds are then described in Section III. The particle identification (PID) to select electrons from muons in the PØD is a key component of this measurement, and will be described further in the section on event selection. The water subtraction method is then described in IV. The detector, reconstruction, flux and cross section systematic uncertainties in the measurement are reviewed in Section V. Finally the results of the rate measurement are presented in Section VI and a summary is in Section VII.

## II.  ND280 $\pi^0$ DETECTOR

The T2K ND280 $\pi^0$ Detector (PØD) is a scintillator based tracking calorimeter optimized to measure neutral current $\pi^0$ in the momentum range that contributes to backgrounds for $\nu_e$ appearance [13]. We refer the reader to Fig. 4 of [13] for a picture of the PØD detector. The PØD is composed of layers of plastic scintillator alternating with water targets and brass sheets or lead sheets. The PØD sits in front of a tracking detector made up of two fine grain scintillator modules which serve as active targets placed between three time projection chambers. Both the PØD and tracking detector are surrounded by electromagnetic calorimeters and are in a 0.2 T magnetic field.

The PØD is constructed using 40 scintillator modules, each module is constructed with two perpendicular arrays of triangular scintillating bars and is approximately 38 mm thick. The scintillator modules are arranged in three regions. The most upstream and downstream regions of the detector are composed of seven modules in-

TABLE I. Summary of T2K runs and the number of protons on target (POT) used in the analysis.

| T2K run | PØD Config. | Beam Power (kW) | POT ($\times 10^{19}$) |
|---|---|---|---|
| Run I | Water | 50 | 2.96 |
| Run II | Water | 120 | 6.96 |
| Run II | Air | 120 | 3.59 |
| Run III | Air | 178 | 13.5 |
| Run IV | Water | 178 | 16.5 |
| Run IV | Air | 178 | 17.8 |
| Total | Water | | 26.4 |
| | Air | | 34.9 |

terleaved with 4.5 mm thick sheets of stainless steel-clad lead that function as 4.9 radiation length electromagnetic calorimeters to improve the containment of photons and electrons. The central region serves as a target containing water. It has 25 water target layers that are 28 mm thick sandwiched between 26 scintillator modules and 1.3 mm brass sheets, positioned in between water targets and scintillator layers. The target region has a fiducial mass of approximately 1900 kg of water and 3570 kg of other materials.

The energy resolution of the PØD can be estimated from Monte Carlo studies by calculating the difference between true and reconstructed energy for many events. The energy resolution for electrons after the selections described in III, is 16%.

## III.  EVENT SELECTION

### A.  Overview

In this analysis, all the data collected between January 2010 and May 2013 except for very small fraction of Run III data, due to the magnetic horn current decrease which caused a failure in good spill pre-selection, are used. The data are subdivided into different run periods and PØD configurations as shown in Table I. The simulated data used in this analysis corresponds to ten times the Protons on Target (POT) of the data, and reproduces the various experimental conditions of the different data-taking periods.

Neutrino interactions in ND280 are simulated with the NEUT [1] event generator, version 5.1.4.2. The generator covers a range of neutrino energy from several tens of MeV to hundreds of TeV and simulates all the nuclear targets present in ND280. In the simulated data, neutrino interactions are generated outside and within the full ND280 volume including all active and inactive material, providing information to understand the signal and backgrounds from interactions outside the ND280 fiducial volume. The details of the simulation process are described in [23].

Simulation of products of the neutrino interactions in the PØD is done using a GEANT 4.9.4 simulation [24–

27]. The standard GEANT physics list for electromagnetic interactions is used in the simulation.

The analysis uses two reconstructed objects, a track and a shower. Within the PØD reconstruction algorithm, hits in PØD scintillator layer associated with a reconstructed track classified as an electromagnetic track (typically electrons or photons) are forwarded to the shower reconstruction stage. Hits associated with a track that are classified as a light track (typically muon) or a heavy track (typically proton) are not forwarded to the shower reconstruction stage and cannot be reconstructed as a shower.

The signal events for the analysis are the charged current $\nu_e$ interactions in the PØD. A cut-based event selection using known reconstruction characteristics was tuned to maximize the product of efficiency and purity. To avoid bias, the selection strategy was developed based on Monte Carlo (MC) samples. Event displays of a typical CC$\nu_e$ candidate and a $\pi^0$ background event selected in the analysis are shown in Fig. 1.

## B. Selection Cuts

The event selection strategy focuses on identifying single high-energy electron shower events with a vertex in the PØD. As a pre-selection, the reconstructed shower in the PØD must be in time with the beam bunch time. The PØD reconstruction searches for both tracks and showers with two independent algorithms, and the highest energy track and the highest energy shower are used in the analysis. The reconstruction algorithm builds tracks and showers from hits, but as the shower reconstruction occurs after the track reconstruction we need to make sure that the hits shower reconstruction uses are the same hits the track reconstruction uses, for each single event. Therefore we require 80% of the hits associated with the track and shower to be the same.

In addition, we select events where the angle of the reconstructed shower with respect to the z-axis, which is approximately the beam axis, is less than 45°. The scintillator bars of the PØD have a triangular profile with angles of approximately 45°. Particles with an angle of more than 45° with respect to the beam axis would therefore hit more than two adjacent bars in a layer. The PØD reconstruction algorithm currently only handles up to two adjacent bar hits in a layer, causing reconstruction failures for higher angle tracks.

For this analysis, only events with a reconstructed neutrino energy of 1.5 GeV or more are selected. Reconstructed neutrino energy is calculated from the reconstructed electron energy and the electron angle using the quasi-elastic approximation. In this energy region, the majority of the $\nu_e$ flux arises from kaon decays and the PØD shows good performance to distinguish electrons from other particles. In addition, using a high neutrino energy cut improves the purity of the electron sample.

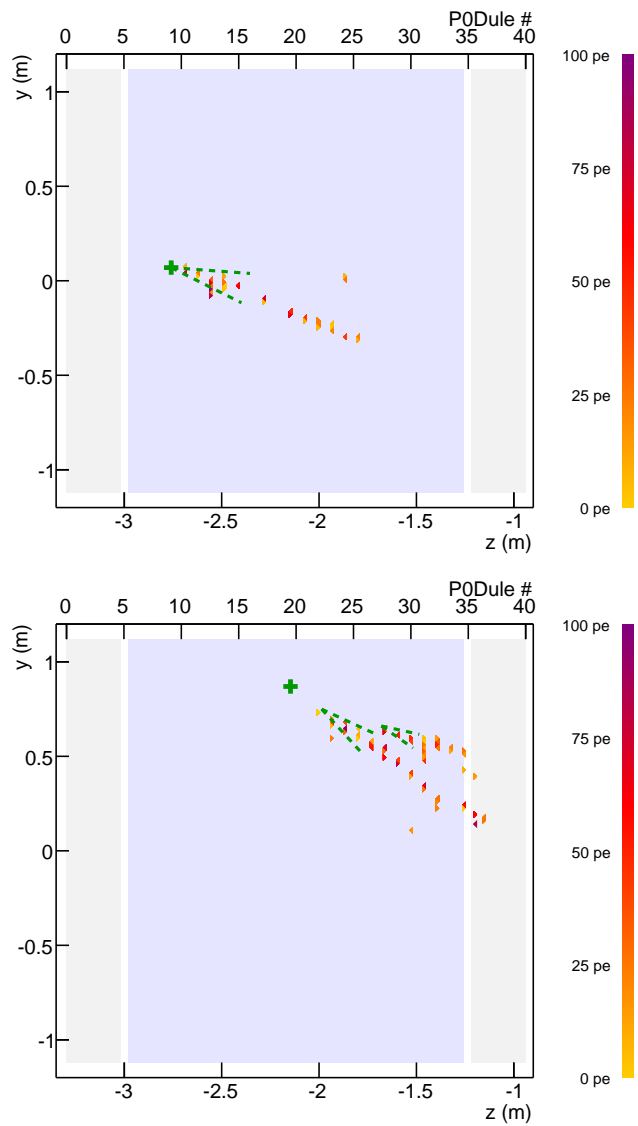To reject muons, the median width of the selected



FIG. 1. Side view of a CC$\nu_e$ event (top) and a $\pi^0$ background event (bottom) reconstructed in the PØD. Triangles are hits colored by the charge deposited, the green cross symbol shows the reconstructed shower vertex, and the green dashed lines show the cones of reconstructed showers.

track is used. In each scintillator layer, the energy-weighted standard deviation of the position of the hits reconstructed in the track is calculated as follows:

1. If the two hits with the highest deposited energy are in adjacent strips, replace them with a single hit. The new hit's position is at the energy-weighted average position of the two original hits, and its energy is the sum of the energies of the original hits. Any other hits in the layers are left unchanged. This procedure gives layers with minimum ionizing tracks very small (almost always zero) width.

2. The energy-weighted standard deviation of the hit positions is calculated for each layer.
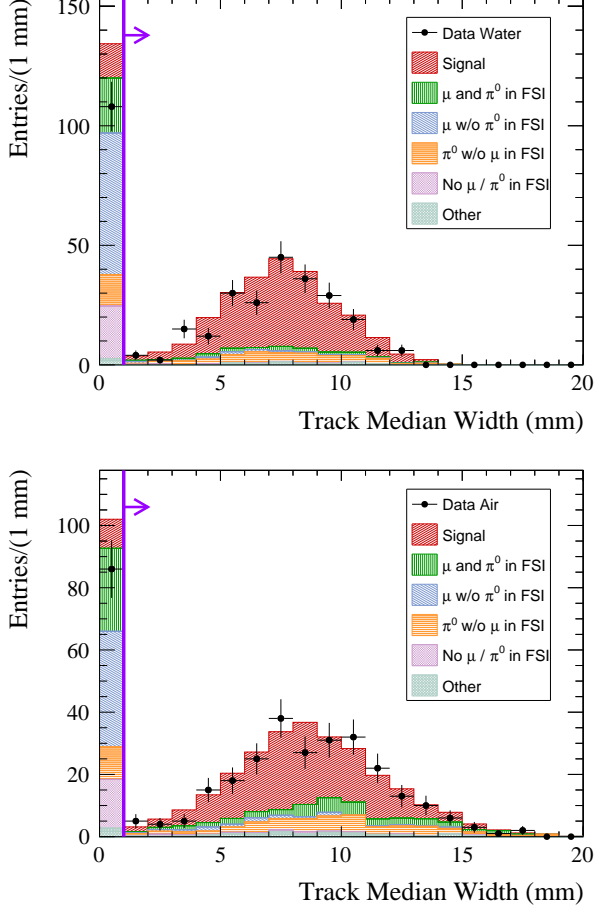
FIG. 2. Distribution of events which pass all the selection criteria with the exception of the track median width cut, for water (top) and air configuration (bottom). The vertical line shows the cut value used (1 mm). A sudden drop of events above 11 mm is an effect of shower median width cut.
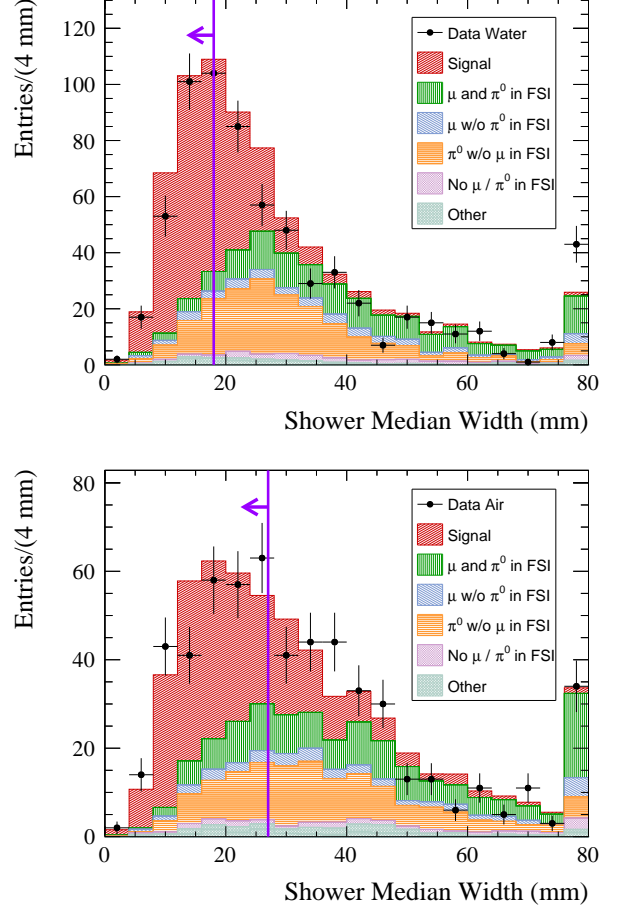


FIG. 3. Distribution of events which pass all the selection criteria with the exception of the shower median width cut, for water (top) and air configuration (bottom). The vertical line shows the applied cuts which are optimized for each configuration.

   3. Median width is the width of the middle layer after ordering by layer width.

   The design of the PØD with layers of high density materials (brass and lead) causes electrons to shower. The reconstructed track of an electron is therefore typically wider than the reconstructed track of a muon. This feature can be used to distinguish muons and electrons with the median width of the reconstructed candidate track.

   The track median width for events which pass all the selection criteria with the exception of the track median width cut, is shown in Fig. 2 and indicates that most of the background muon events are rejected by this cut.

   Similarly, to reject background events that contain neutral pions, a cut is applied to the median width of the selected shower. The shower reconstruction looks for hits in a cone from the reconstructed vertex position and combines them in one or more showers. It can happen that hits from several particles are combined in one reconstructed shower, especially when they are almost overlap-ping. The PØD $\nu_e$ analysis looks for events with a single electron. Events with a very wide candidate shower are rejected, because such events are more likely background events with several particles. The shower median width is calculated the same way as the track median width. Distributions of events which pass all the selection criteria with the exception of the shower median width cut is shown in Fig. 3. It shows many $\pi^0$ background events are rejected with this cut.

   Finally, a cut is applied to the fraction of the event's charge that is contained in the selected shower. To select CC$\nu_e$ events with a high purity, we require that the fraction of the event's charge contained in the candidate shower is exactly 1.0, selecting only events with a single shower and without muon-like tracks in final state.

TABLE II. The selected number of MC signal events, MC background events, and the total number of selected MC events normalized to data POT for water and air configuration are listed together with the selected data events. In addition, the water configuration MC events are split up in on-water and not-water events. The errors correspond to the statistical uncertainty due to the limited MC statistics.

|  | MC Signal | MC Background | MC Total | Data |
|---|---|---|---|---|
| Water | $196.1 \pm 4.8$ | $56.7 \pm 2.7$ | $252.8 \pm 5.5$ | 230 |
| On-Water | $60.2 \pm 2.6$ | $14.5 \pm 1.3$ | $74.7 \pm 2.9$ | |
| Not-Water | $135.9 \pm 4.0$ | $42.2 \pm 2.3$ | $178.2 \pm 4.6$ | |
| Air | $173.6 \pm 4.6$ | $97.4 \pm 3.6$ | $271.0 \pm 5.8$ | 257 |

TABLE III. The signal efficiencies $\epsilon$ and purities $p$ are listed for water and air configuration. Events of the PØD water configuration are split into events happening on-water and not-water. The errors correspond to the statistical uncertainty due to the limited MC statistics.

|  | Efficiency $\epsilon$ | Purity $p$ |
|---|---|---|
| Water | $(10.9 \pm 0.3)\%$ | $(77.6 \pm 2.5)\%$ |
| On-Water | $(9.8 \pm 0.4)\%$ | $(80.6 \pm 4.7)\%$ |
| Not-Water | $(11.5 \pm 0.4)\%$ | $(76.3 \pm 3.0)\%$ |
| Air | $(11.0 \pm 0.3)\%$ | $(64.1 \pm 2.2)\%$ |

### C. Selected Event Samples

The selected number of events passing all cuts predicted by the simulation, both when the PØD is configured to contain water and air, together with the number of selected data events are presented in Table II. The water configuration simulation events are separated into on-water and not-water events. On-water events are defined as events with true interaction vertex in the water, and not-water events have the true interaction vertex on scintillator, lead, brass, or other materials besides water. All events in the air configuration MC are not-water events as the water targets are drained.

### D. Efficiency and purity

The efficiency $\epsilon$ and purity $p$ of the simulated electron neutrino signal events, for water and air configurations, are summarized in Table III. In the PØD water configuration, events are split into events happening on water (on-water) and events on scintillator, brass, and lead (not-water).

The selection efficiency of signal events as function of the true neutrino energy $E_{\text{true}}$ for PØD water and air configurations are shown in Fig. 4. The selection of low energy signal events is suppressed by the high neutrino energy cut at 1.5 GeV while the selection of high energy signal events is suppressed by the shower median width cut and the shower charge fraction cut.
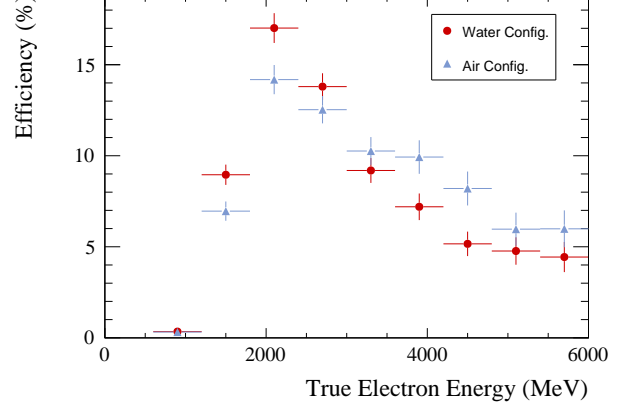


FIG. 4. Selection efficiency of signal events as function of the true neutrino energy $E_{\text{true}}$ for water and air configuration. The error bars correspond to the uncertainties due to limited MC statistics.

### IV. WATER SUBTRACTION METHOD

The measured $\nu_e$ interactions that were collected during PØD water and air configuration running are compared with the number of $\nu_e$ interactions predicted by the PØD water and air configuration MC, respectively. The measured number of $\nu_e$ interactions are extracted by subtracting the predicted MC background $B$ from the selected data events $D$, resulting in:

$$N^{Data}_{CC\nu_e,\text{water}} = D_{\text{water}} - B_{\text{water}}, \text{ and} \qquad (1)$$

$$N^{Data}_{CC\nu_e,\text{air}} = D_{\text{air}} - B_{\text{air}}. \qquad (2)$$

The background subtracted data are then divided by the predicted Monte Carlo signal $S$ to obtain the data/MC ratios for the water and air configurations:

$$R_{\text{water}} = \frac{N^{Data}_{CC\nu_e,\text{water}}}{S_{\text{water}}}, \text{ and} \qquad (3)$$

$$R_{\text{air}} = \frac{N^{Data}_{CC\nu_e,\text{air}}}{S_{\text{air}}}. \qquad (4)$$

To extract the measured number of on-water charged current $\nu_e$ interactions, the measured $CC\nu_e$ interactions with PØD water and air configurations are compared by taking into account the different collected POT and the different reconstruction efficiencies for the water and the air data sample using:

$$N^{Data}_{CC\nu_e,\text{on-water}} = (D_{\text{water}} - B_{\text{water}})$$
$$- \frac{\epsilon_{\text{not-water}} \cdot \text{POT}_{\text{water}}}{\epsilon_{\text{air}} \cdot \text{POT}_{\text{air}}} \cdot (D_{\text{air}} - B_{\text{air}}). \qquad (5)$$

In this formula, $\text{POT}_{\text{water}} = 2.64 \times 10^{20}$ ($\text{POT}_{\text{air}} = 3.49 \times 10^{20}$) is the collected data POT for the PØD water (air) configuration. The resulting data/MC ratio for on-water $\text{CC}\nu_e$ interactions is given by:

$$R_{\text{on-water}} = \frac{N_{\text{CC}\nu_e,\text{on-water}}^{Data}}{S_{\text{on-water}}}. \tag{6}$$

## V. SYSTEMATIC UNCERTAINTIES

The systematic uncertainties in the measurements are divided into three categories: detector, reconstruction, and neutrino flux/cross section uncertainties. Control sample events to study systematic effects in the measurement have been studied, but often the events in these control samples are not used for the final systematic uncertainty evaluation. The control sample events were found to be too similar to the signal events, or did not have the same background as the signal events. For this reason a simple KS test is used for several of the systematic uncertainty tests, particularly where no deviation is indicated in the test.

### A. Detector systematic uncertainties

The detector's as-built mass and its mass in the Monte Carlo are different. The masses for water and air configurations as well as different run periods also vary. These differences are incorporated in the analysis procedure by re-weighting MC events with mass uncertainties estimated to be 0.01 for all configurations. Similarly, the fiducial volume and the alignment of the PØD is considered. Varying the fiducial volume by the MC vertex resolution and shifting in PØD alignment provides an estimate of the systematic uncertainties in data/MC ratios. The uncertainties obtained are smaller than 0.01 for all ratios making them negligible in this measurement.

Possible systematic effects on the reconstructed electron energy are also studied. The effects are investigated by changing the reconstructed energy scale to observe the differences in $\text{CC}\nu_e$ data/MC ratios. The possible effects are as follows: 1. PØD material density and thickness, 2. drifts in the PØD response over time, and 3. the simulation (GEANT4) uncertainty in the electron energy deposition. We assume the water and air configuration are correlated for the PØD material density and thickness only. The resulting systematic uncertainties for water ($R_{\text{water}}$), air ($R_{\text{air}}$), and on-water ($R_{\text{on-water}}$) are 0.05, 0.05, and 0.10 respectively.

### B. Reconstruction systematic uncertainties

#### 1. Track PID

As described earlier at the beginning of Section III, the classification of the reconstructed tracks is based on the PØD PID. Differences in the PID between data and MC can therefore cause systematic uncertainties in the $\text{CC}\nu_e$ data/MC ratios.

A PID study with stopping muons in the PØD was performed to estimate this uncertainty, and a map of mis-PID between a data sample and a simulation of stopping muons was constructed. To estimate the impact of the track PID uncertainty on the $\text{CC}\nu_e$ data/MC ratios, the MC signal and background was weighted according to the uncertainty of the map. The systematic parameter values were randomly varied assuming that the water and air samples are uncorrelated and also that the signal and background uncertainties are uncorrelated. The uncertainties for water ($R_{\text{water}}$), air ($R_{\text{air}}$), and on-water ($R_{\text{on-water}}$) were determined to be 0.05, 0.05, and 0.09 respectively.

#### 2. Track and Shower Median width

To estimate the systematic uncertainty caused by the track median width, the plots with all selection criteria applied but failing the track median width cut (the N-1 plots) are integrated, and a Kolmogorov-Smirnov test is performed to test if the data and the Monte Carlo event distributions are consistent[28, 29]. The Kolmogorov-Smirnov test returns a p-value of 91.2% for water and 92.2% for air configuration indicating that there are no significant evidence for a shift between the data and MC event distributions. The systematic uncertainty due to the track median width cut is therefore negligible for this analysis.

The threshold of the shower median width cut is placed in a region with a large number of events. The systematic uncertainty on the measured shower median width therefore has a larger impact on the $\text{CC}\nu_e$ data/MC ratios than the track median width uncertainty does. To estimate the systematic uncertainty caused by the shower median width, the N-1 plots are integrated, and a Kolmogorov-Smirnov test is performed. The Kolmogorov-Smirnov test returns a p-value of 50.0% for water and 65.9% for air configuration. To determine a reasonable scaling factor range for Monte Carlo, different scaling factors from 0.9 to 1.1 were applied to Monte Carlo and the resulting p-values were studied. For a p-value of 68%, the peak scaling factor ranged from 0.98 to 1.02. The systematic effect on the $\text{CC}\nu_e$ data/MC ratios for $R_{\text{water}}$, $R_{\text{air}}$, and $R_{\text{on-water}}$ coming from the shower median width are estimated by varying the scaling factor that is applied to the MC shower median width. The uncertainties obtained for $R_{\text{water}}$, $R_{\text{air}}$, and $R_{\text{on-water}}$ are 0.04, 0.04, and 0.08 respectively.

### 3. Shower Charge Fraction

To estimate the possible impact of systematic effects of the shower charge fraction on the analysis, additional reconstructed objects with low energy are studied. Such additional tracks or showers would cause an event to fail the shower charge fraction selection criteria. Looking at the event distribution of these events, the only hint for a systematic difference between data and MC appears in the highest bin of the air configuration. Events with a shower charge fraction between 0.98 and 1.00 which pass all other selection criteria are analyzed to estimate the systematic uncertainty. The data/MC difference in this region is considered to be the uncertainty on the MC events in the signal region, resulting in the systematic uncertainties for $R_{\text{water}}$, $R_{\text{air}}$, and $R_{\text{on-water}}$ of 0.01, 0.04, and 0.04 respectively.

### C. Flux and cross section systematic uncertainties

For the inclusion of the flux and cross section systematic uncertainties in the analysis, each analyzed MC event is re-weighted according to the uncertainties of the flux and cross section parameters which are correlated. The parameter values and uncertainties are provided by different external measurements such as NA61 and other hadronic production experiments, and these parameters are then fitted to ND280 data from TPC and FGD, the other subdetectors of ND280 than PØD. The systematic parameters and their uncertainties obtained from the fit to the ND280 data, which includes 25 flux parameters, 6 FSI parameters, 2 NEUT parameters, and 13 neutrino interaction parameters, has been studied in Ref. [23].

To obtain the flux and cross section systematic uncertainties, the systematic parameters are thrown according to the covariance matrix and the analysis described in Section IV is then applied to each throw. The distributions are fit with single Gaussians and the resulting width is considered to be the flux and cross section systematic uncertainty for the analysis. The uncertainties obtained for water ($R_{\text{water}}$), air ($R_{\text{air}}$), and on-water ($R_{\text{on-water}}$) are 0.07, 0.09, and 0.06 respectively.

### D. Summary of the systematic uncertainties

All systematic uncertainties on the CC$\nu_e$ data/MC ratios for water ($R_{\text{water}}$), air ($R_{\text{air}}$), and on-water ($R_{\text{on-water}}$) that were estimated in the previous sections are summarized in Table IV. This table also shows the total systematic uncertainty.

### VI. RESULTS

The results obtained for the background subtracted data/MC ratio ($R$) for water configuration, air configu-

TABLE IV. Summary of systematic uncertainties on the CC$\nu_e$ data/MC ratios for water ($R_{\text{water}}$), air ($R_{\text{air}}$), and on-water ($R_{\text{on-water}}$).

| Systematic Uncertainty | $R_{\text{water}}$ | $R_{\text{air}}$ | $R_{\text{on-water}}$ |
|---|---|---|---|
| MC Statistics | 0.03 | 0.04 | 0.12 |
| PØD Mass | 0.01 | 0.01 | 0.01 |
| PØD Fiducial Volume | < 0.01 | < 0.01 | < 0.01 |
| PØD Alignment | < 0.01 | < 0.01 | < 0.01 |
| Energy Scale | 0.05 | 0.05 | 0.10 |
| Hit Matching | < 0.01 | < 0.01 | < 0.01 |
| Track PID | 0.05 | 0.05 | 0.09 |
| Energy Resolution | < 0.01 | < 0.01 | 0.01 |
| Angular Resolution | < 0.01 | < 0.01 | 0.01 |
| Track Median Width | < 0.01 | < 0.01 | < 0.01 |
| Shower Median Width | 0.04 | 0.04 | 0.08 |
| Shower Charge Fraction | 0.01 | 0.04 | 0.04 |
| Flux and Cross Sections | 0.07 | 0.09 | 0.06 |
| Total | 0.11 | 0.13 | 0.21 |

ration, and on-water are:

$$R_{\text{water}} = 0.89 \pm 0.08 \text{ (stat.)} \pm 0.11 \text{ (sys.)}, \quad (7)$$

$$R_{\text{air}} = 0.90 \pm 0.09 \text{ (stat.)} \pm 0.13 \text{ (sys.)}, \text{ and} \quad (8)$$

$$R_{\text{on-water}} = 0.87 \pm 0.33 \text{ (stat.)} \pm 0.21 \text{ (sys.)}. \quad (9)$$

The ratios are consistent with 1, within statistical and systematic uncertainties. For the on-water ratio, uncertainties are relatively large due to limited statistics and the impact of the subtraction method.

For the selected events, the distribution of the reconstructed particle directions is shown in Fig. 5 and the distribution of particle energies is shown in Fig. 6. This result indicates that the beam $\nu_e$ component in high energy region measured in the data is consistent with expectations after including constraints from the ND280 data for all configurations.

### VII. CONCLUSION

In conclusion, measurements of CC$\nu_e$ interactions using the ND280 PØD have been made. The PØD includes fillable water targets which allows separate measurements for the water and air configurations of the ND280 PØD as well as the measurement of $\nu_e$ on-water interactions above 1.5 GeV in a predominantly $\nu_\mu$ beam. About $\sim85\%$ of the selected sample comes from the decay of kaons.

The 230 (257) water configuration (air configuration) electron neutrino candidate events selected in the data are in good agreement with the prediction for the water configuration, the air configuration, and for the on-water subtraction samples respectively. The measurement is statistically limited, especially for on-water, but it will be improved in the future as we plan to collect ten times
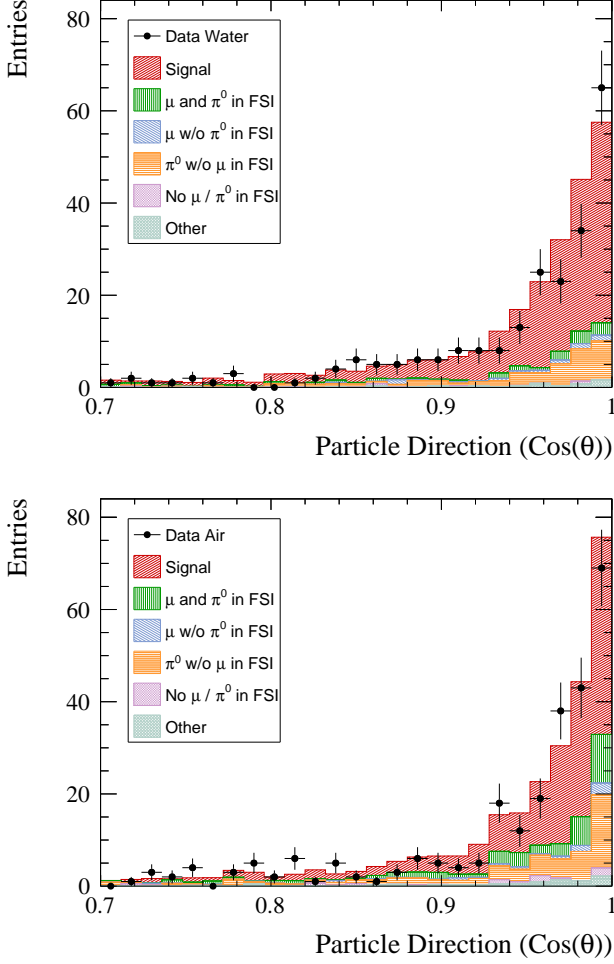
FIG. 5. Events passing the event selection as a function of the particle direction for water (top) and air configuration (bottom). The MC events are normalized to data POT, and the fit results from ND280 are applied.
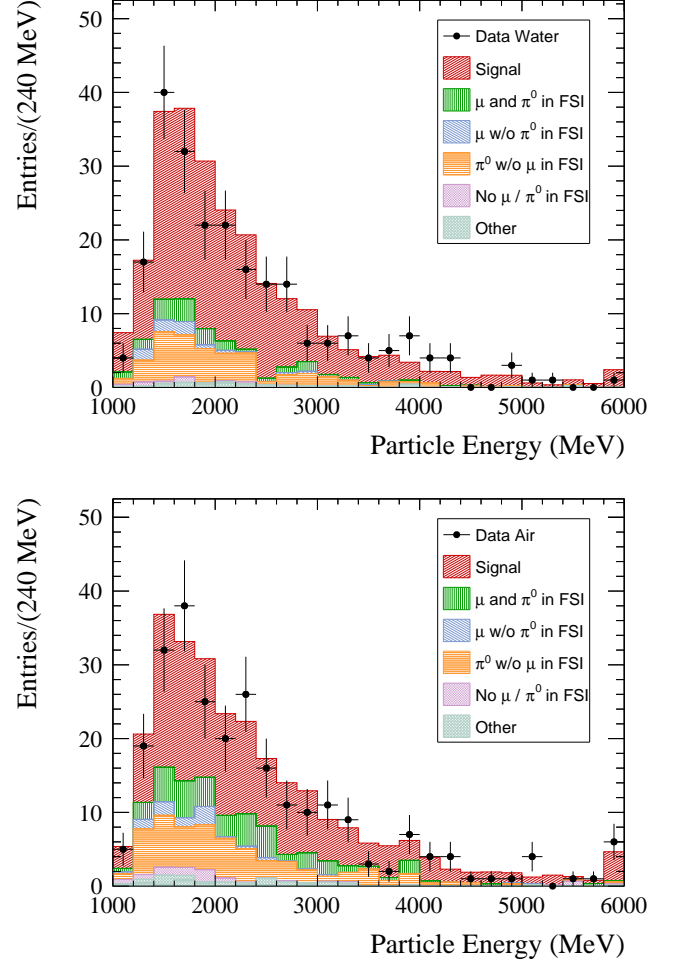


FIG. 6. Events passing the event selection as a function of the particle energy for water (top) and air configuration (bottom). The MC events are normalized to data POT, and the fit results from ND280 are applied.

more data in the coming years. Furthermore, studies and improvements to the reconstruction algorithms are being investigated to lower the energy threshold, which will lead to the measurement of the $\nu_e$ cross section on water.

This is the first $\nu_e$ interaction rate measurement on water in the few GeV energy region. Interactions of $\nu_e$ on water are of particular interest for long-baseline neutrino oscillation experiments, and atmospheric neutrino experiments using water Cherenkov detectors with the aim to measure $CP$ violation in the lepton sector. Above all, this is the first measurement of $\nu_e$ interaction rate on water in the few GeV energy region.

[1] Y. Hayato, Nuclear Physics B - Proceedings Supplements **112**, 171 (2002).

[2] J. Blietschau *et al.* (Gargamelle), Nucl. Phys. **B133**, 205 (1978).

[3] L. B. Auerbach *et al.* (LSND), Phys. Rev.D **63**, 112001 (2001), arXiv:hep-ex/0101039.

[4] J. A. Formaggio and G. P. Zeller, Rev. Mod. Phys. **84**, 1307 (2012).

[5] K. Abe *et al.* (T2K Collaboration), Nucl.Instrum.Meth. **A659**, 106 (2011), arXiv:1106.1238 [physics.ins-det].

[6] J. Arafune *et al.*, Phys. Rev. D **56**, 3093 (1997).

[7] K. Abe *et al.* (T2K Collaboration), Phys.Rev.Lett. **112**, 061802 (2014), arXiv:1311.4750 [hep-ex].

[8] K. Abe *et al.* (T2K Collaboration), Phys. Rev. D **87**, 012001 (2013).

[9] K. Abe *et al.*, "Letter of Intent: The Hyper-Kamiokande Experiment, Detector Design and Physics Potential," (2011), arXiv:1109.3262 [hep-ex].

[10] C. Adams *et al.* (LBNE Collaboration), "Scientific Opportunities with the Long-Baseline Neutrino Experiment," (2013), arXiv:1307.7335 [hep-ex].

[11] A. Stahl *et al.*, "Expression of interest for a very long baseline neutrino oscillation experiment (LBNO)," CERN-PH-EP-2012-021, SPSC-EOI-007 (2012).

[12] K. Abe *et al.* (T2K collaboration), Phys. Rev. D **89** (2014), arXiv:1403.2552 [hep-ex].

[13] S. Assylbekov *et al.* (T2K ND280 P0D Collaboration), Nucl.Instrum.Meth. **A686**, 48 (2012).

[14] B. G. Tice *et al.* (Minerva), Phys. Rev. Lett **112**, 23181 (2014), arXiv:1403.2103 [hep-ex].

[15] B. Tice, *Measurement of Nuclear Dependence in Inclusive Charged Current Neutrino Scattering*, Ph.D. thesis, Rutgers University (2014).

[16] M. Day and K. S. McFarland, Phys. Rev. D **86**, 053003 (2012).

[17] G. Zeller, Chinese Physics C **38**, 526 (2014).

[18] G. Gran *et al.*, Phys. Rev. D **74**, 052002 (2006).

[19] C. Mariani *et al.*, Phys. Rev. D **83**, 054023 (2011).

[20] A. Rodriguez *et al.*, Phys. Rev. D **78**, 032003 (2008).

[21] S. Nakayama *et al.*, Phys. Rev. Lett. **619**, 255 (2005).

[22] M. Hasegawa *et al.*, Phys. Rev. Lett. **95**, 252301 (2005).

[23] K. Abe *et al.* (The T2K Collaboration), Phys. Rev. D **89**, 092003 (2014).

[24] A. Schalicke *et al.*, J. Phys: Conf. Ser. **331** (2011).

[25] O. Kadri *et al.*, Nucl. Instrum. Meth **B258**, 381 (2007).

[26] D. L. Sawkey and B. A. Faddegon, Med Phys. **36(3)**, 698 (2009).

[27] V. N. Ivanchenko, Nucl. Instrum. Meth **A502**, 666 (2003).

[28] A. Kolmogorov, G. Ist. Ital. Attuari **4**, 8391 (1933).

[29] N. Smirnov, Annals of Mathematical Statistics **19**, 279281 (1948).